Efficient fifth harmonic generation of Nd:glass laser in ADP crystals

Fang Wang (王 芳), Xuewei Deng (邓学伟), Liquan Wang (王礼权), Fuquan Li (李富全), Wei Han (韩 伟), Wei Zhou (周 维), Xiaoxia Huang (黄小霞), Huaiwen Guo (郭怀文), and Qihua Zhu (朱启华)*

Research Center of Laser Fusion, China Academy of Engineering Physics, Mianyang 621999, China
**Corresponding author: qhzh@163.com*

Received May 29, 2019; accepted July 19, 2019; posted online November 26, 2019

Fifth harmonic generation (5th HG) of a Nd:glass laser is an effective way to acquire high-energy coherent deep-ultraviolet radiation near 200 nm. In this work, cascade generation of the fifth harmonic of a Nd:glass laser in a 5 mm ammonium dihydrogen phosphate (ADP) crystal was investigated, and maximum conversion efficiency of 14% and large angular acceptance of 45 mrad were demonstrated at a noncritical phase-matching temperature of −75.1°C. However, as the results reveal, the temperature sensitivity and nonlinear absorption would hinder its high-energy application. As for that, based on the complementary relationship of the angle and temperature in the phase-matching condition, an upgraded focusing 5th HG design coupled with the cylindrical temperature distribution scheme was proposed. By this upgraded focusing design, more than the improvement of the conversion efficiency, the output 5ω near-field intensity distribution turns out to be insensitive to the temperature gradient. Potentially, this idea can be applied for many other frequency conversion schemes such as high-repetition frequency lasers, which have similar temperature gradient problems.

OCIS codes: 140.3610, 140.3515, 190.2620.
doi: 10.3788/COL201917.121403.

Deep-ultraviolet (DUV) coherent light sources near 200 nm are extensively required for science, medicine, and industrial applications[1,2]. Especially, in the context of high-energy-density physics, DUV lasers are desirable for probing beams of diagnostics such as Thomson scattering diagnostic devices[3–6]. The higher-frequency probe laser has better penetration of the dense plasma and can reduce the background due to plasma emission, as well as suppress the absorption, refraction, and dispersion of the probe laser in the plasma. It is well known that the fifth harmonic generation (5th HG) of a Nd:glass laser is an effective way to acquire coherent DUV radiation near 200 nm. Nevertheless, in most available materials with the high UV transmission, the large dispersion at short wavelengths can hardly be compensated by their birefringence, resulting in dissatisfying the 5th HG's phase-matching condition. In previous reports, beta-barium borate (β-BBO)[7,8] and cesium lithium borate (CLBO) crystals[9–11] were commonly used to generate the fifth harmonic (5ω). Nevertheless, the BBO crystal suffers from a large walk-off angle and limited size, while the CLBO crystal is restricted for its easy hygroscopicity and creaking. Although the potassium dihydrogen phosphate (KDP) crystal can be used to generate the 5th harmonic by mixing the fundamental frequency and the 4th harmonic of a 1053 nm laser, the phase-matching temperature of about −140°C[12] would cost too much.

The ammonium dihydrogen phosphate (ADP) crystal[13–17] may be a good choice for efficient 5th HG of the Nd:glass laser. It is available in large sizes and exhibits relatively high damage resistance and nonlinearity with an acceptable UV transmission cutting edge below 200 nm. Most importantly, the noncritical phase-matching (NCPM) condition can be satisfied above the liquid nitrogen temperature. However, 5th HG of the 1055 nm laser with ADP crystals was reported as early as several decades ago[17], and further investigation can rarely be seen. There was no description of either the influences of angular and temperature aberrations on conversion efficiency, or the reported NCPM temperatures of −70°C. Moreover, there is a big difference in the NCPM temperatures between the experimental result of −70°C and the calculated value of −50.7°C according to the simulation by the Select Non-Linear Optics (SNLO) software from Sandia National Lab. On the other hand, according to the temperature-dependent Sellmeier formula of ADP crystal[18], the temperature matching condition is very rigorous, and it would be a restriction for its practical application[19–21]. In this Letter, first we investigate the temperature and angular tuning characteristics of 5th HG of the Nd:glass laser in ADP crystals, and then we propose an upgraded focusing 5th HG scheme with cylindrical temperature distribution to improve the 5th HG performance.

The experimental setup for 5th HG is shown in Fig. 1. A neodymium-doped yttrium lithium fluoride (Nd:YLF) laser was used, whose wavelength is 1053 nm. The repetition rate is 1 Hz; the maximum output energy is about 10 mJ; the pulse width is 50 ps; the beam spot size is 5 mm in diameter. Three nonlinear crystals were employed for the experiments. The first crystal, which is a 5 mm long, type I 90°-cut lithium triborate (LBO) crystal, converted the fundamental wave (1ω) to its second harmonic (2ω). The second crystal, which is an 8.3 mm long, type I 79°-cut

 © 2019 Chinese Optics Letters

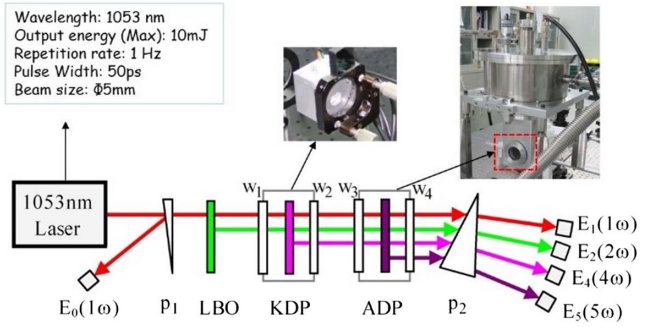

Fig. 1. Experimental setup of NCPM 5th HG of a 1053 nm laser. Photos of the thermostat for the 4th HG and 5th HG crystals are also shown in the figure.

KDP crystal, housed in an oven with a working temperature of 24.0°C, converted the 2ω laser into the fourth harmonic (4ω). The third crystal, a rapid-grown, type I 90°-cut ADP crystal with the size of 15 mm × 15 mm× 5 mm, produced the 5ω by mixing the residual 1ω laser and the generated 4ω laser. A thermostatically controlled Dewar, which contained liquid nitrogen, a heater, a thermistor sensor, and the controller, and a vacuum system were adopted to maintain the ADP crystal at a certain temperature within its operating range. Four DUV windows were mounted on the two sides of the 4th HG and the 5th HG crystals, respectively, for temperature controlling. Two wedges were used for energy measurement, in which p_1 served for the input 1ω energy sampling, and p_2 served for the harmonics separation. All of the nonlinear crystals and their accessory optics were fine polished, but only the LBO crystal was anti-reflective coated. Five calibrated identical energy calorimeters (Geotec QE25LP-S-MB) were employed to measure the input and output laser energies.

To measure the NCPM temperature for 5th HG of the 1053 nm laser in the ADP crystal, experiments were carried out with input 1ω intensity of 0.6 GW/cm^2, while the readings of the calorimeters were moderate. Before the experiments, the temperature equilibrium was kept for more than 10 h, and the vacuum degree was maintained at 0.4 Pa to isolate the heat conduction by air. Besides, the crystal and the sensor fixed to the metallic holder were well polished to lessen the thermal resistance. Thus, we deduce that the experimental error is comparatively small. Figure 2 shows the normalized $1\omega \rightarrow 5\omega$ conversion efficiency tuning curve as a function of crystal temperature. The red squares indicate the measured data, and the black curve is the calculated result by referencing the SNLO software and the Sellmeier equations in literature[18]. The accurate NCPM temperature (T_{NCPM}) was fitted to be −75.1°C, which basically agrees with the reported result in literature[17] rather than the calculated value. We think that the calculation deviation should be attributed to the refractive index deviations of the empirical refractive index equations in the DUV band and the large weight factor of the 5ω light in the

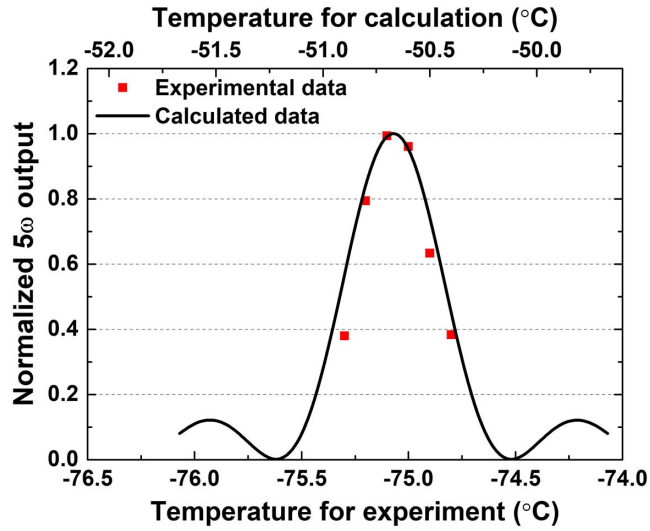

Fig. 2. Measured (red squares) and calculated (black curve) temperature tuning characteristics for NCPM 5th HG of the 1053 nm laser.

phase-matching relationship, so it should be revised. The full width at half-maximum (FWHM) temperature bandwidth was found to be 0.45°C, which is in accordance with the theoretical simulation. The temperature acceptance yields a bandwidth of 0.225°C · cm by the given 5 mm length of the ADP crystal.

Figure 3 shows the measured angular tuning curves with input 1ω intensity of 0.6 GW/cm^2, and the black squares, red circles, and blue triangles indicate crystal temperatures of −75.3°C, −75.2°C, and −75.1°C, respectively. When the working temperature is lower than T_{NCPM}, the phase-matching condition can be achieved again by adjusting the incident angle. There are two phase-matching angles symmetrically distributed around the collimated position (the detuned angle is specified to be 0 mrad in Fig. 3), where the 5ω wave vector is strictly vertical to the crystal optical axis. By optimizing the working temperature, the two adjacent angles link

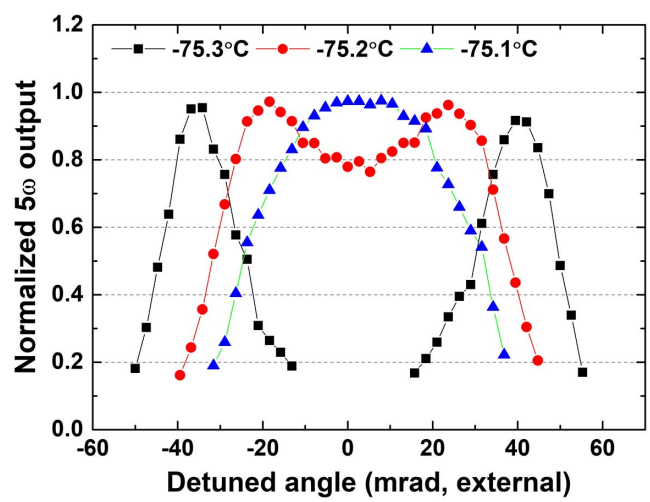

Fig. 3. Measured angular tuning curves at different working temperatures for 5th HG of the 1053 nm laser.

together, and the FWHM angular bandwidth increases to be about 45 mrad. By the 5 mm length of the ADP crystal, the angular acceptance yields a bandwidth of 22.5 mrad · cm.

To assess the potential of ADP for 5th HG application, experiments were carried out with the crystal collimated and the working temperature fixed at −75.1°C. The 1ω-to-5ω conversion efficiency is defined as E_5/E_0, and the tuning curve versus the input 1ω energy and intensity is shown in Fig. 4(a). The maximum efficiency is about 14%, which is not actually high due to several factors. First, the optics except the LBO crystal were all uncoated. Second, the thickness of the frequency conversion crystals was not optimized but chosen for their availability in our laboratory. Third, as Fig. 4(b) shows, the non-uniform near-field distribution should also decrease the efficiency. In practical applications, the above problems should be solved to improve the 5th HG efficiency. The main trouble limiting the efficiency of the 5th HG process would be the two-photon absorption (TPA) loss of DUV radiations[22], which can be illustrated by the energy balance experiments, as Fig. 4(c) shows. The energy balance is defined as the total energies at different wavelengths measured after p_2 is divided by the input 1ω energy E_0. The optical frequency in the subscript (e.g., $B_{4\omega}$) indicates the maximum frequency presented in the measurement, that is, $B_{4\omega}$ was measured with the 5th HG crystal completely detuned. It is easy to see that, as the intensity increases, the nonlinear losses of 4ω and 5ω light turn out to be significant. The energy balance at low intensities was only 56%, primarily caused by the losses from uncoated optical surfaces.

Since the nonlinear loss is the intrinsic problem of the materials, it can only be suppressed by lowering the 5ω radiation power density. That means the beam apertures have to be increased, and the temperature uniformity controlling becomes very difficult. For this reason, in the following part, we give a focusing design proposal coupled with the cylindrical temperature distribution to relieve this problem.

The main idea of the focusing 5th HG design is to use the large angular acceptance to compensate for the phase mismatching induced by inhomogeneous temperature distribution. In this design, a focusing lens is inserted before the 5th HG crystal, and the temperature gradient within the crystal aperture can be compensated by optimizing the focal length of the focusing lens. As we know, the phase-matching factor is a function of multiple parameters, including angle, temperature, wavelength, and so on. That is to say, the phase mismatching caused by any one parameter can be compensated for by the others. Figure 5 exhibits the complementation of temperature and angular aberrations for the phase-matching relationship indicated by a factor of $\mathrm{sinc}^2(\Delta kL/2)$, where Δk is the phase mismatching, and L is the crystal length. As we can see, when the working temperature is lower than the NCPM temperature, the phase-matching condition can be satisfied again by adjusting the incident angle. There are two phase-matching angles symmetrically distributed around $\theta = 90°$, and these two adjacent angles are joined together at the NCPM temperature. These conclusions are consistent with the experimental results referred to in Fig. 3.

The feasibility and compensation effect of our design mainly depend on the temperature distribution in the crystal. For the transmission optics, the surrounded clamping and conduction structure are commonly used. Since the thermal chamber is not absolutely heat insulated nor absolute vacuum, the heat exchange from the crystal surface cannot be avoided, and the temperature gradient would always exist. Obviously, the temperature uniformity control of the transmission optics turns much more difficult for a larger radius–thickness ratio and lower vacuum degree. Fortunately, the temperature distribution with such a structure is always slow-varying and symmetric, which makes the phase-mismatching compensation feasible. Moreover, for the 5th HG process in ADP crystal, the NCPM temperature is much lower than the room temperature, which means that the central temperature would be higher than the perimeter zones. When the

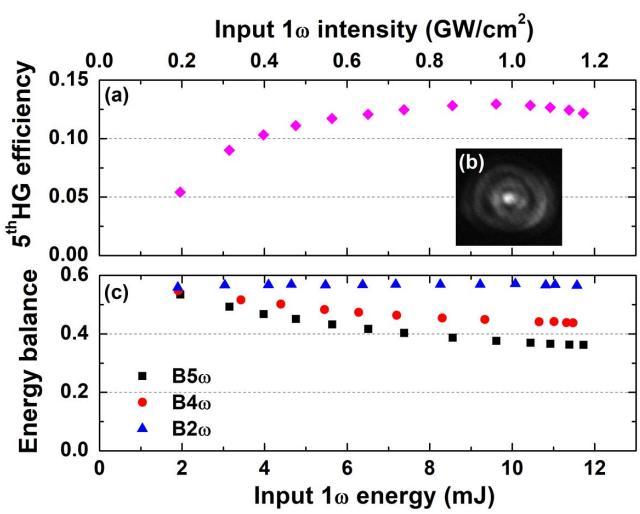

Fig. 4. (a) Fifth-harmonic efficiency and (c) energy balance measured as a function of input pulse energy and intensity. The near-field pattern of the output 5ω radiation is also shown in inset figure (b).

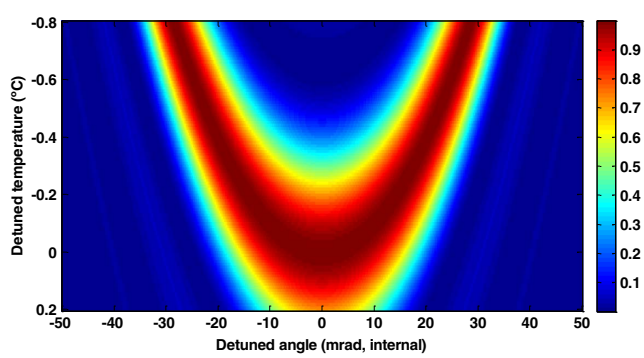

Fig. 5. Phase-matching factor $\mathrm{sinc}^2(\Delta kL/2)$ as a function of angle and temperature.

central temperature satisfies the NCPM condition, the phase mismatching due to a lower temperature around the perimeter zones is possible to be compensated for by the convergence angle of the focusing beam. Furthermore, the temperature compensation by the convergent angle is only needed along the sensitive axis direction of the crystal. So, a cylindrical temperature distribution similar to a tile is proposed to solve this problem, with the square crystal surround clamped, but only thermally conducted by two edges along the non-sensitive axis direction.

To verify the advantage of this focusing design, we conducted the numerical simulations. Firstly, the temperature distributions with the traditional central-symmetric thermal controller and upgraded cylindrical-symmetric thermal controller were simulated by the COMSOL software. Crystal parameters in simulation were chosen according to engineering issues. For probe beam of several tens of Joules with low damage risk, the crystal size was defined as 120 mm × 120 mm. For the trade-off between reducing absorption and decreasing the processing, together with clamping difficulties, the thickness was defined to be 5 mm. The central temperature was set to be −75.1°C, and the air pressure was set to be 0.4 Pa which can be easily realized in the laboratory. The simulating results for the two conduction manners are shown in Figs. 6(a) and 6(b), respectively.

The numerical model of the 5th HG process was developed by solving the nonlinear coupled wave equations using the split-step Fourier algorithm[23,24]. In this model, besides the three-wave coupling process, the effects such as diffraction, transverse walk-off, linear and nonlinear absorption were included. The SHG and 4th HG crystal types and thicknesses were set as the same as those used in our experiments, and the input 1ω intensity was specified to be 0.8 GW/cm^2 to avoid overloaded nonlinear absorption. The effective nonlinearity coefficient of ADP crystal was assumed to be 0.79 pm/V, and the TPA coefficients were assumed to be $\beta_{45} = 1.0$ cm/GW, $\beta_{55} = 2.0$ cm/GW. The crystal thickness was set to be 5 mm, as referred to above. The spatial distribution of the input beam was in the eighth super-Gaussian, with dimensions of 80 mm × 80 mm. For simplicity, the pulse temporal profile was set to be a 1 ns flat top beam.

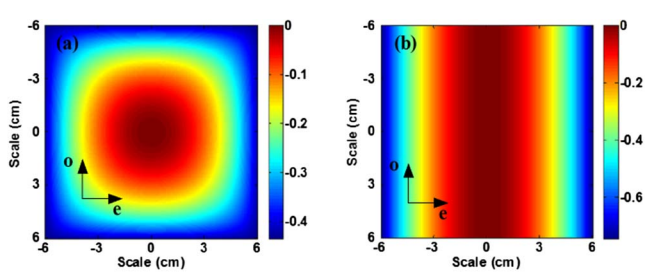

Fig. 6. Simulated temperature distributions of a 120 mm × 120 mm × 5 mm ADP crystal in (a) the traditional scheme and (b) the focusing design. The central temperature is set to be −75.1°C. The color bars indicate the temperature deviation.

Generally, the phase-matching condition can hardly be satisfied over the whole crystal due to the temperature gradient distribution of the traditional scheme. Fortunately, the conversion efficiency can be optimized by changing the focal length of the focusing lens for the focusing design. As shown in Fig. 7, with the above input parameters, the maximum conversion efficiency can be achieved when the focal length is 1.45 m.

More than the improving of the conversion efficiency, the output 5ω near-field intensity distribution turns out to be insensitive to the temperature gradient. Figure 8 shows the near-field distribution before and after optimized compensation, while the traditional scheme used temperature optimization, and the focusing design adopted angular compensation by changing the focusing length. The inset Figs. 8(a) and 8(b) represent the situation of the traditional scheme, and Figs. 8(c) and 8(d)

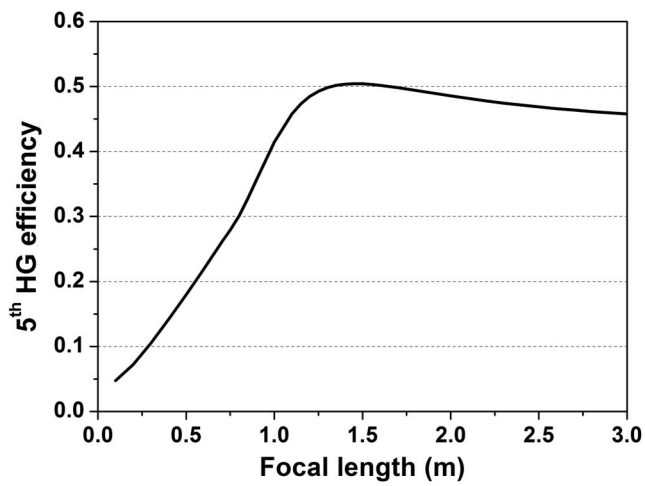

Fig. 7. 5th HG efficiency optimization with the focal length of the focusing lens for the upgraded focusing design.

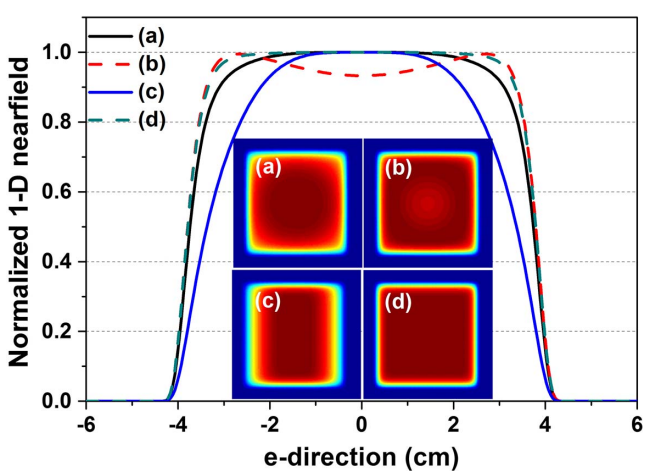

Fig. 8. 5ω near-field distribution (a), (c) before and (b), (d) after compensation. Inset figures (a) and (b) represent the situation of the traditional scheme, figures (c) and (d) represent the situation of the upgraded scheme, and the curves are the corresponding 1D profiles.

represent the situation of the upgraded scheme, and the curves are the corresponding one-dimensional (1D) profiles. As can be seen, the near-field degradation around the perimeter can hardly be compensated in the traditional scheme, while in the focusing design the near-field can almost be compensated. This is because the temperature gradient distribution of the upgraded scheme is uniform along the sensitivity direction of the crystal, so the lower temperature around the perimeter zones can be well compensated by the convergence angle of the focusing beam.

We also investigated the influence of beam center deviation on 5th HG efficiency and output 5ω near-field. Obviously, the focusing scheme will perform better when the beam offsets along the o axis because the temperature distribution in this direction is almost uniform. So, our simulations only focus on the situation that the beam offsets along the e direction, and the results are shown in Fig. 9. The black and red curves indicate the influence of beam offsetting on 5th HG efficiency for the traditional scheme and the focusing design, respectively. It can be seen that the influence of transverse deviation rarely affects the conversion efficiency of the focusing scheme since the complementary relationship of the angle and temperature has greatly increased the phase-matching acceptance range in this direction. The near-field degradation can nearly be neglected, as shown in the insets (d), (e), and (f) of Fig. 9. Conversely, both efficiency decreasing and near-field degradation are obvious as the transverse deviation increases in the insets of (a), (b), and (c) of Fig. 9. To sum up, the transverse deviations, whether along the o direction or the e direction, rarely deteriorate the performance of the focusing scheme.

In conclusion, with a −75.1°C temperature controlled ADP crystal, we realized high-efficiency NCPM 5th HG of a Nd:glass laser. The maximum optical conversion efficiency reached 14%, which can be increased by optimizing the crystal length, decreasing the component Fresnel losses, and improving the beam near-field uniformity. The angular and the temperature acceptance bandwidths were measured to be 22.5 mrad · cm and 0.225°C · cm, respectively. An upgraded focusing 5th HG design was proposed, and the conflicts among high output energy, lower TPA effect, and extreme temperature sensitivity can be relieved. In this new design, the phase mismatching induced by the inhomogeneous temperature distribution can almost be compensated by the angular detuning of the focused laser beam. The theoretical analysis manifests that it can bring higher conversion efficiency, as well as superior near-field intensity distribution, which will benefit practical applications. Furthermore, this idea may provide a new way for frequency conversion schemes such as high-repetition frequency lasers, which are troubled by temperature gradient problems.

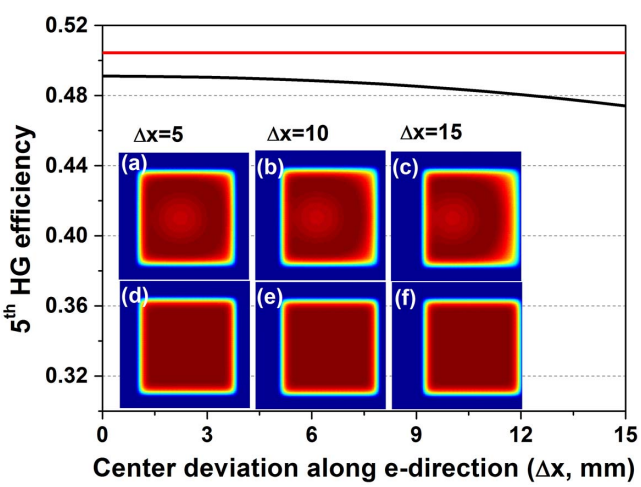

Fig. 9. Influence of beam center deviation along the e direction on 5th HG conversion efficiency (curves) and 5ω near-field distribution (insets). The black curve along with figures (a), (b), and (c) represents the situation of the traditional scheme, and the red curve along with figures (d), (e), and (f) represents the situation of the focusing design.

This work was supported by the National Natural Science Foundation of China (Nos. 11704352, 61805223, and 61775199).

References

1. S. Mao, Y. Li, J. Jiang, S. Shen, and K. Liu, Chin. Opt. Lett. **16**, 030801 (2018).
2. K. Wang, C. Gong, D. Zou, X. Jin, and Z. Xu, Chin. Opt. Lett. **15**, 040602 (2017).
3. J. S. Ross, J. L. Kline, S. Yang, M. Henesian, T. Weiland, D. Price, B. B. Pollock, and S. H. Glenzer, Rev. Sci. Instrum. **81**, 10D524 (2010).
4. V. V. Ivanov, A. A. Anderson, and I. A. Begishev, Appl. Opt. **55**, 498 (2016).
5. J. S. Ross, S. H. Glenzer, J. P. Palastro, B. B. Pollock, D. Price, G. R. Tynan, and D. H. Froula, Rev. Sci. Instrum. **81**, 10D523 (2010).
6. P. Datte, J. S. Ross, D. Froula, J. Galbraith, S. Glenzer, B. Hatch, J. Kilkenny, O. Landen, A. M. Manuel, W. Molander, D. Montgomery, J. Moody, J. Nelson, J. Weaver, G. Vergel de Dios, and M. Vitalich, in *Ninth International Conference on Inertial Fusion Sciences and Applications* (2015), paper Th.Po.4.
7. A. Dubietis, G. Tamošauskas, A. Varanavicius, G. Valiulis, and R. Danielius, Opt. Soc. Am. B **17**, 48 (2000).
8. A. Dubietis, G. Tamošauskas, A. Varanavičius, G. Valiulis, and R. Danielius, Opt. Lett. **25**, 1116 (2000).
9. Y. K. Yap, M. Inagaki, S. Nakajima, Y. Mori, and T. Sasaki, Opt. Lett. **21**, 1348 (1996).
10. J. Sakuma, Y. Asakawa, T. Imahoko, and M. Obara, Opt. Lett. **29**, 1096 (2004).
11. I. A. Begishev, in *Conference on Lasers and Electro-Optics*, OSA Technical Digest (2016), paper SM3M.1.
12. A. G. Akmanov, S. A. Akhmanov, B. V. Ahdanov, A. I. Kovrigin, N. K. Podsotskaya, and R. V. Khokhlov, J. Exp. Theor. Phys. Lett. **10**, 154 (1969).
13. D. N. Nikogosyan, *Nonlinear Optical Crystals: A Complete Survey* (Springer, 2005).
14. S. Ji, F. Wang, L. Zhu, X. Xu, Z. Wang, and X. Sun, Sci. Rep. **3**, 1605 (2013).
15. J. Reintjes and R. C. Eckardt, Appl. Phys. Lett. **30**, 91 (1977).
16. G. A. Massy, Appl. Phys. Lett. **24**, 371 (1974).

17. I. A. Begishev, R. A. Ganeev, A. A. Gulamov, E. A. Erofeev, Sh. R. Kamalov, T. Usmanov, and A. D. Hadzhaev, Sov. J. Quantum Electron. **18**, 224 (1988).
18. A. Richard Phillips, J. Opt. Soc. Am **56**, 629 (1966).
19. G. Naveen, J. Electromag. Waves Appl. **32**, 2350 (2018).
20. G. Naveen, Laser Part. Beams **37**, 184 (2019).
21. D. Tang, J. Wang, B. Zhou, G. Xie, J. Ma, P. Yuan, H. Zhu, and L. Qian, J. Opt. Soc. Am. B **34**, 1659 (2017).
22. A. Dubietis, G. Tamošauskas, A. Varanavičius, and G. Valiulis, Appl. Opt. **39**, 2437 (2000).
23. P. W. Milonni, J. M. Auerbach, and D. Eimerl, Proc. SPIE **2633**, 230 (1995).
24. P. J. Wegner, J. M. Auerbach, C. E. Barker, S. C. Burkhart, S. A. Couture, J. J. DeYoreo, R. L. Hibbard, L. W. Liou, M. A. Norton, P. K. Whitman, and L. A. Hackel, Proc. SPIE **3492**, 392 (1999).